only *OCT4* and *SOX2*, rendering *CMYC* and *KLF4* dispensable and thereby reducing the oncogenic potential of the resulting cells. Furthermore, our findings enabled *CMYC* and *KLF4*-free iPSC production without inhibition of p53 or its target genes involved in apoptosis, allowing pro-apoptotic pathways that ensure genomic integrity to be engaged [8,10,11]. Thus, in this approach, the production of oncogene-free iPSC lines does not come at the expense of an increase in mutational load [8,10,11,45].

Studies using nuclear transplantation and defined transcription factors have shown that nuclei become less amenable to reprogramming as they advance developmentally [24-26]. Our study demonstrates that intercellular communication in somatic cultures can cause them to differentiate and lose their reprogramming potential, but that with small molecule treatment, it is possible to force them to remain in an undifferentiated, highly reprogrammable state. This approach synergized potently with chemical inactivation of the histone H3 methyltransferase DOT1L, allowing two-factor reprogramming at higher efficiency than with four transcription factors. This indicates that while histone methyltransferase inhibition had almost no effect on the reprogramming of differentiated keratinocytes, it had a profound ability to enhance the reprogramming of undifferentiated keratinocytes. Thus, somatic cells at different developmental stages respond differentially to chromatin-modifying signals during reprogramming. The combined chemical inhibition of NOTCH and DOT1L provides a new approach for boosting the reprogramming potential of keratinocytes and is an attractive starting point for the identification of a small molecule reprogramming cocktail for human cells.

Online Methods

iPSC reprogramming experiments

The IACUC committee of Harvard University approved the use of mice for all experiments included in this paper. *Oct4*:GFP neonatal mouse keratinocytes were isolated from P1-P2 pups using an overnight digestion in either .25% trypsin/EDTA or TrypLE (Life Technologies) at 4 degrees Celsius. They were cultured in SFM medium (Life Technologies) on collagen IV-coated plates. Neonatal human epidermal keratinocytes (Lonza) were cultured in Epilife medium (Invitrogen) on collagen-coated plates. Keratinocytes were reprogrammed using retroviruses containing either mouse or human *OCT4, SOX2, KLF4*, and *CMYC* produced in the pMXs backbone. Chemical treatment was initiated 1-2 days after viral transduction and re-administered every other day until the end of the experiment unless otherwise specified. DAPT (EMD Millipore) was used at 10 μM for reprogramming experiments using *OCT4, SOX2, KLF4*, and *CMYC* and 2.5 μM for *OCT4, SOX2* reprogramming experiments unless otherwise noted. DBZ was used at 2 μM. Irradiated mouse embryonic fibroblast feeders were added 6 days after transduction and the media was changed to mouse or human embryonic stem cell medium at that time. Colonies were scored as iPSC colonies if they were *Oct4*::GFP+ in mouse experiments or NANOG+/ TRA-1-81+ in human experiments.

Gene expression analysis of iPSCs

Nanostring (Nanostring Technologies) and scorecard analysis was performed as described [34]. iPSCs were cultured in mTesr1 medium (Stem Cell Technologies) prior to RNA isolation. To measure their differentiation propensities, iPSCs were dissociated into embryoid bodies and cultured in human embryonic stem cell medium without bFGF for 16 days. Cells were then lysed and total RNA was extracted using Trizol (Life Technologies) and purified using the RNeasy kit (QIAGEN). 300 ng to 500 ng of RNA was profiled on the Nano-String nCounter system (Nanostring Technologies) according to manufacturer's instructions. A custom nCounter codeset covering 500 genes that monitor cell state, pluripotency, and differentiation was used [34]. Data analysis was performed with the R statistics package as in [34]. Briefly, the lineage scorecard performs a parametric gene set enrichment analysis on t scores obtained from a pairwise comparison between the cell line of interest and the reference of ES cell-derived EBs.

Differentiation of iPSCs

For teratoma formation, 1-2 million human iPSCs were injected into the kidney capsule of nude mice and harvested 2 months later. Teratomas were sectioned and stained with hematoxylin and eosin for visualization. For the mouse iPSC chimera assay, 10 *Oct4*::GFP+ iPSCs were injected per ICR blastocyst, and 20 blastocysts were transplanted into each pseudopregnant female. Embryos were either allowed to develop to term or harvested at day E12.5 and dissected for genital ridge analysis using a stereomicroscope.

Gene expression analysis of reprogramming cultures

Illumina MouseRef-8 microarrays (Illumina) were used for genome-wide mRNA expression analysis of reprogramming mouse keratinocyte cultures treated with DMSO or 10 μM DAPT. For QPCR analysis, RNA was isolated using Trizol, cDNA synthesis was performed using the iScript cDNA synthesis kit (Bio-rad), and the SYBR Green qPCR Supermix (Bio-rad) was used for PCR product detection.

Western blots and immunofluorescence

Antibodies detecting mouse Notch (Santa Cruz Biotechnology, sc-6015), human NOTCH (Abcam, ab27526, and Santa Cruz Biotechnology, sc-23307), cleaved human NOTCH (Cell Signaling Technology, 2421), p53 (Santa Cruz Biotechnology, sc-56182), Involucrin (Abcam, Ab53112), and p21 (Cell Signaling Technology 05-345) were used for western blots. Blots were quantified using ImageJ software. Antibodies specific for NANOG (Abcam, AF1997) and TRA-1-81 (Chemicon, MAB4381) were used to identify human iPSCs. A γH2AX (Abcam, ab11175) antibody was used to detect γH2AX foci. Cells in which γH2AX staining covered greater than half the nucleus were scored as positive for γH2AX foci.

UV irradiation assay

UV irradiation was performed at a dosage of 30 J. TUNEL staining was performed using a TUNEL kit (Pharmacia Biosciences).

shRNA/siRNA knockdown experiments

shRNAs and siRNAs were purchased from Sigma and added to reprogramming cultures within 1 day after addition of the reprogramming retroviruses. shRNAs (TRCN0000003753, p53 and TRCN0000287021, p21) were expressed in the pLKO.1 lentiviral backbone. siRNAs were used at 80nM and were transfected into reprogramming cultures using RNAiMAX (Life Technologies).

Array CGH analysis of iPSC lines

Cell Line Genetics performed array CGH analysis of iPSC lines at passage 5 using 4×180K +SNP analysis.

Statistical analysis

For all experiments, error bars represent the standard deviation between two-three biological replicates and statistical significance was determined using a two-tailed homoscedastic Student's t-test.

Supplementary Material

Refer to Web version on PubMed Central for supplementary material.

Acknowledgements

The authors would like to thank E. Son for assistance with microarray data analysis, S. Sato for assistance with chimera experiments, E. Kiskinis for assistance with nanostring analysis, and K. Koszka and M. Yamaki for assistance with teratoma experiments. The authors are grateful for the financial support that made this work possible. K.E. was supported by NIH R01 grant 5 R01 GM96067-03, NIH P01 grant GM099117 and HHMI. A.M was supported by NIH P01 grant GM099117. H.A. was supported by grants from the Ministry of Education, Culture, Sports, Science and Technology (MEXT) of Japan, Grant-in-aid for Scientific Research (21390456) and Grant-in-Aid for challenging Exploratory Research (22659304), and a grant from JST-CREST. J.K.I. was supported by a Stan and Fiona Druckenmiller/New York Stem Cell Foundation postdoctoral fellowship, NIH K99 grant 1K99NS077435-01A1, NIH R00 grant 4R00NS077435-03, and the Novartis Institutes for BioMedical Research. C.B. was supported by a Feodor Lynen Fellowship from the Alexander von Humboldt Foundation.

References

1. Aoi T, et al. Generation of Pluripotent Stem Cells from Adult Mouse Liver and Stomach Cells. Science. 2008; 321:699–702. [PubMed: 18276851]
2. Nakagawa M, et al. Generation of induced pluripotent stem cells without Myc from mouse and human fibroblasts. Nat Biotechnol. 2008; 26:101–6. [PubMed: 18059259]
3. Kawamura T, et al. Linking the p53 tumour suppressor pathway to somatic cell reprogramming. Nature. 2009; 460:1140–4. [PubMed: 19668186]
4. Okita K, et al. A more efficient method to generate integration-free human iPS cells. Nat Methods. 2011; 8:409–12. [PubMed: 21460823]
5. Son MJ, et al. Nicotinamide overcomes pluripotency deficits and reprogramming barriers. Stem Cells. 2013; 31:1121–35. [PubMed: 23526681]
6. Hong H, et al. Suppression of induced pluripotent stem cell generation by the p53-p21 pathway. Nature. 2009; 460:1132–5. [PubMed: 19668191]
7. Utikal J, et al. Immortalization eliminates a roadblock during cellular reprogramming into iPS cells. Nature. 2009; 460:1145–8. [PubMed: 19668190]
8. Marion RM, et al. A p53-mediated DNA damage response limits reprogramming to ensure iPS cell genomic integrity. Nature. 2009; 460:1149–53. [PubMed: 19668189]

9. Li H, et al. The Ink4/Arf locus is a barrier for iPS cell reprogramming. Nature. 2009; 460:1136–9. [PubMed: 19668188]
10. Li Y, et al. The p53-PUMA axis suppresses iPSC generation. Nat Commun. 2013; 4:2174. [PubMed: 23873265]
11. Lake BB, et al. Context-dependent enhancement of induced pluripotent stem cell reprogramming by silencing Puma. Stem Cells. 2012; 30:888–97. [PubMed: 22311782]
12. Guo S, et al. Nonstochastic reprogramming from a privileged somatic cell state. Cell. 2014; 156:649–62. [PubMed: 24486105]
13. Lee YL, et al. Sirtuin 1 facilitates generation of induced pluripotent stem cells from mouse embryonic fibroblasts through the miR-34a and p53 pathways. PLoS One. 2012; 7:e45633. [PubMed: 23029150]
14. Brosh R, et al. p53 counteracts reprogramming by inhibiting mesenchymal-to epithelial transition. Cell Death Differ. 2013; 20:312–20. [PubMed: 22996684]
15. Ye D, et al. MiR-138 promotes induced pluripotent stem cell generation through the regulation of the p53 signaling. Stem Cells. 2012; 30:1645–54. [PubMed: 22696098]
16. Wang J, et al. p53-facilitated miR-199a-3p regulates somatic cell reprogramming. Stem Cells. 2012; 30:1405–13. [PubMed: 22553189]
17. Zhu S, et al. Reprogramming of human primary somatic cells by OCT4 and chemical compounds. Cell Stem Cell. 2010; 7:651–5. [PubMed: 21112560]
18. Silva J, et al. Promotion of reprogramming to ground state pluripotency by signal inhibition. PLoS Biol. 2008; 6:e253. [PubMed: 18942890]
19. Ichida JK, et al. A small-molecule inhibitor of tgf-Beta signaling replaces sox2 in reprogramming by inducing nanog. Cell Stem Cell. 2009; 5:491–503. [PubMed: 19818703]
20. Hou P, et al. Pluripotent stem cells induced from mouse somatic cells by small-molecule compounds. Science. 2013; 341:651–4. [PubMed: 23868920]
21. Huangfu D, et al. Induction of pluripotent stem cells by defined factors is greatly improved by small-molecule compounds. Nat Biotechnol. 2008; 26:795–7. [PubMed: 18568017]
22. Federation AJ, Bradner JE, Meissner A. The use of small molecules in somatic-cell reprogramming. Trends Cell Biol. 2013; 24:179–87. [PubMed: 24183602]
23. Amabile G, Meissner A. Induced pluripotent stem cells: current progress and potential for regenerative medicine. Trends Mol Med. 2009; 15:59–68. [PubMed: 19162546]
24. Eminli S, et al. Differentiation stage determines potential of hematopoietic cells for reprogramming into induced pluripotent stem cells. Nat Genet. 2009; 41:968–76. [PubMed: 19668214]
25. Gurdon JB. The developmental capacity of nuclei taken from intestinal epithelium cells of feeding tadpoles. J Embryol Exp Morphol. 1962; 10:622–40. [PubMed: 13951335]
26. Li J, Greco V, Guasch G, Fuchs E, Mombaerts P. Mice cloned from skin cells. Proc Natl Acad Sci U S A. 2007; 104:2738–43. [PubMed: 17299040]
27. Artavanis-Tsakonas S, Muskavitch MA. Notch: the past, the present, and the future. Curr Top Dev Biol. 2010; 92:1–29. [PubMed: 20816391]
28. Bray SJ. Notch signalling: a simple pathway becomes complex. Nat Rev Mol Cell Biol. 2006; 7:678–89. [PubMed: 16921404]
29. Topley GI, Okuyama R, Gonzales JG, Conti C, Dotto GP. p21(WAF1/Cip1) functions as a suppressor of malignant skin tumor formation and a determinant of keratinocyte stem-cell potential. Proc Natl Acad Sci U S A. 1999; 96:9089–94. [PubMed: 10430900]
30. Missero C, Di Cunto F, Kiyokawa H, Koff A, Dotto GP. The absence of p21Cip1/WAF1 alters keratinocyte growth and differentiation and promotes ras-tumor progression. Genes Dev. 1996; 10:3065–75. [PubMed: 8957006]
31. Aasen T, Belmonte JC. Isolation and cultivation of human keratinocytes from skin or plucked hair for the generation of induced pluripotent stem cells. Nat Protoc. 2010; 5:371–82. [PubMed: 20134422]
32. Aasen T, et al. Efficient and rapid generation of induced pluripotent stem cells from human keratinocytes. Nat Biotechnol. 2008; 26:1276–84. [PubMed: 18931654]

33. Blanpain C, Lowry WE, Pasolli HA, Fuchs E. Canonical notch signaling functions as a commitment switch in the epidermal lineage. Genes Dev. 2006; 20:3022–35. [PubMed: 17079689]
34. Bock C, et al. Reference Maps of Human ES and iPS Cell Variation Enable High-Throughput Characterization of Pluripotent Cell Lines. Cell. 2011; 144:439–52. [PubMed: 21295703]
35. Fuwa H, et al. Divergent synthesis of multifunctional molecular probes to elucidate the enzyme specificity of dipeptidic gamma-secretase inhibitors. ACS Chem Biol. 2007; 2:408–18. [PubMed: 17530731]
36. Nam Y, Sliz P, Song L, Aster JC, Blacklow SC. Structural basis for cooperativity in recruitment of MAML coactivators to Notch transcription complexes. Cell. 2006; 124:973–83. [PubMed: 16530044]
37. Nam Y, Weng AP, Aster JC, Blacklow SC. Structural requirements for assembly of the CSL.intracellular Notch1.Mastermind-like 1 transcriptional activation complex. J Biol Chem. 2003; 278:21232–9. [PubMed: 12644465]
38. Lefort K, Dotto GP. Notch signaling in the integrated control of keratinocyte growth/differentiation and tumor suppression. Semin Cancer Biol. 2004; 14:374–86. [PubMed: 15288263]
39. Jones PH, Watt FM. Separation of human epidermal stem cells from transit amplifying cells on the basis of differences in integrin function and expression. Cell. 1993; 73:713–24. [PubMed: 8500165]
40. Kavian N, et al. Targeting ADAM-17/notch signaling abrogates the development of systemic sclerosis in a murine model. Arthritis Rheum. 2010; 62:3477–87. [PubMed: 20583103]
41. Allen AS, et al. De novo mutations in epileptic encephalopathies. Nature. 501:217–21. [PubMed: 23934111]
42. Huangfu D, et al. Induction of pluripotent stem cells from primary human fibroblasts with only Oct4 and Sox2. Nat Biotechnol. 2008; 26:1269–75. [PubMed: 18849973]
43. Mikkelsen TS, et al. Dissecting direct reprogramming through integrative genomic analysis. Nature. 2008; 454:49–55. [PubMed: 18509334]
44. Onder TT, et al. Chromatin-modifying enzymes as modulators of reprogramming. Nature. 2012; 483:598–602. [PubMed: 22388813]
45. Gore A, et al. Somatic coding mutations in human induced pluripotent stem cells. Nature. 2011; 471:63–7. [PubMed: 21368825]

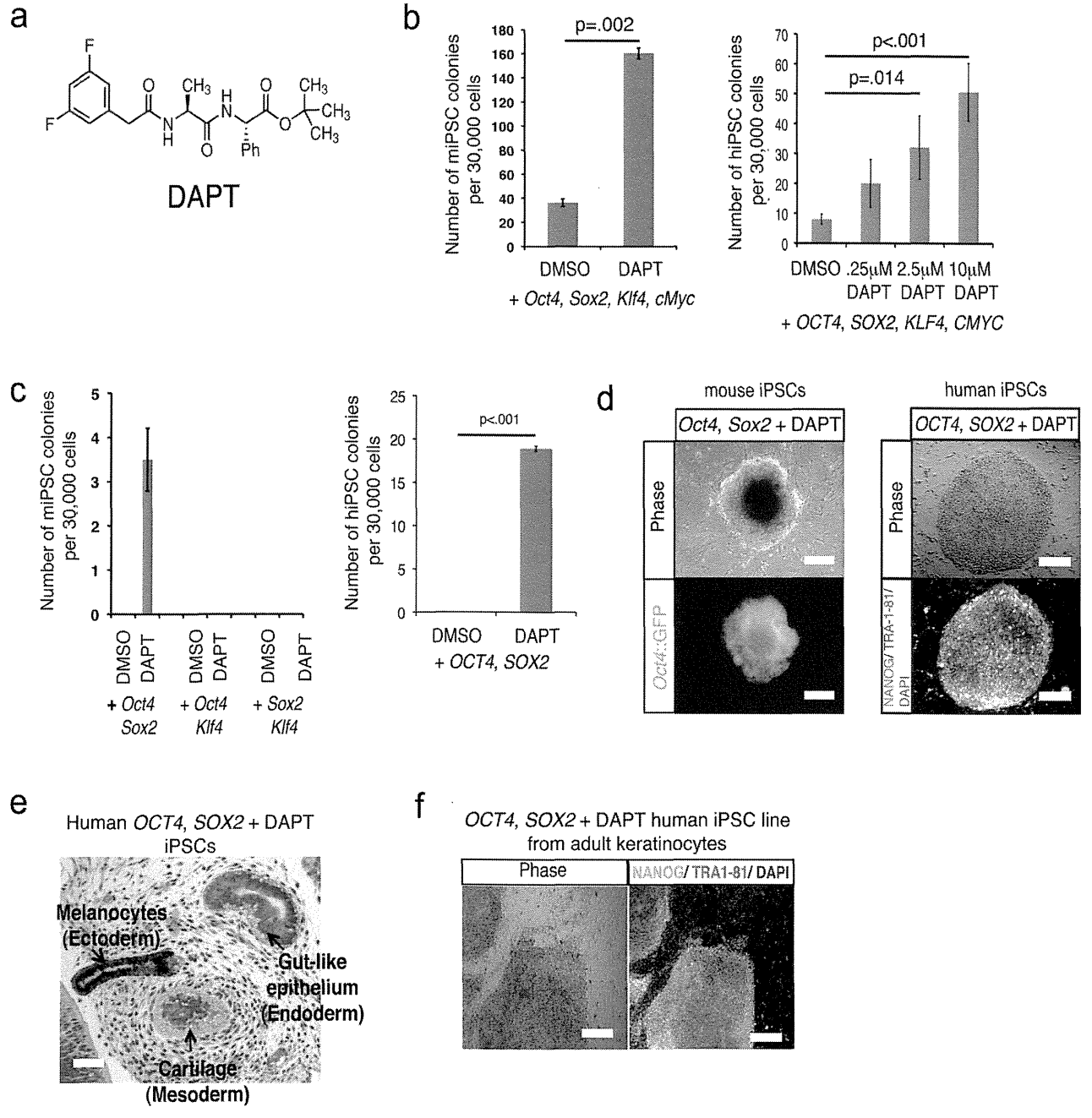

Figure 1. DAPT treatment promotes mouse and human keratinocyte reprogramming

a, Chemical structure of DAPT. **b**, The efficiency of iPSC generation from mouse and human keratinocytes transduced with *Oct4, Sox2, Klf4*, and *cMyc* with DMSO or DAPT treatment (DAPT used at 10 μM in mouse experiment). **c**, The efficiency of iPSC generation from mouse and human keratinocytes transduced with all combinations of 2 reprogramming factors with DMSO or 2.5 μM DAPT treatment from days 1-18 post-transduction. **d**, A P0 mouse and human iPSC colony generated using *OCT4, SOX2*, and DAPT, scale bars = 100 μm. **g**, Teratoma generated by iPSCs derived from human neonatal kerationcytes using *OCT4, SOX2*, and DAPT, scale bar = 50 μm. **j**, NANOG+/TRA-1-81+ iPSC line generated from human adult keratinocytes using *OCT4, SOX2* + DAPT, scale bars = 100 μm. For all experiments, error bars represent the standard deviation between two or three biological

replicates and statistical significance was determined using a two-tailed homoscedastic Student's t-test.

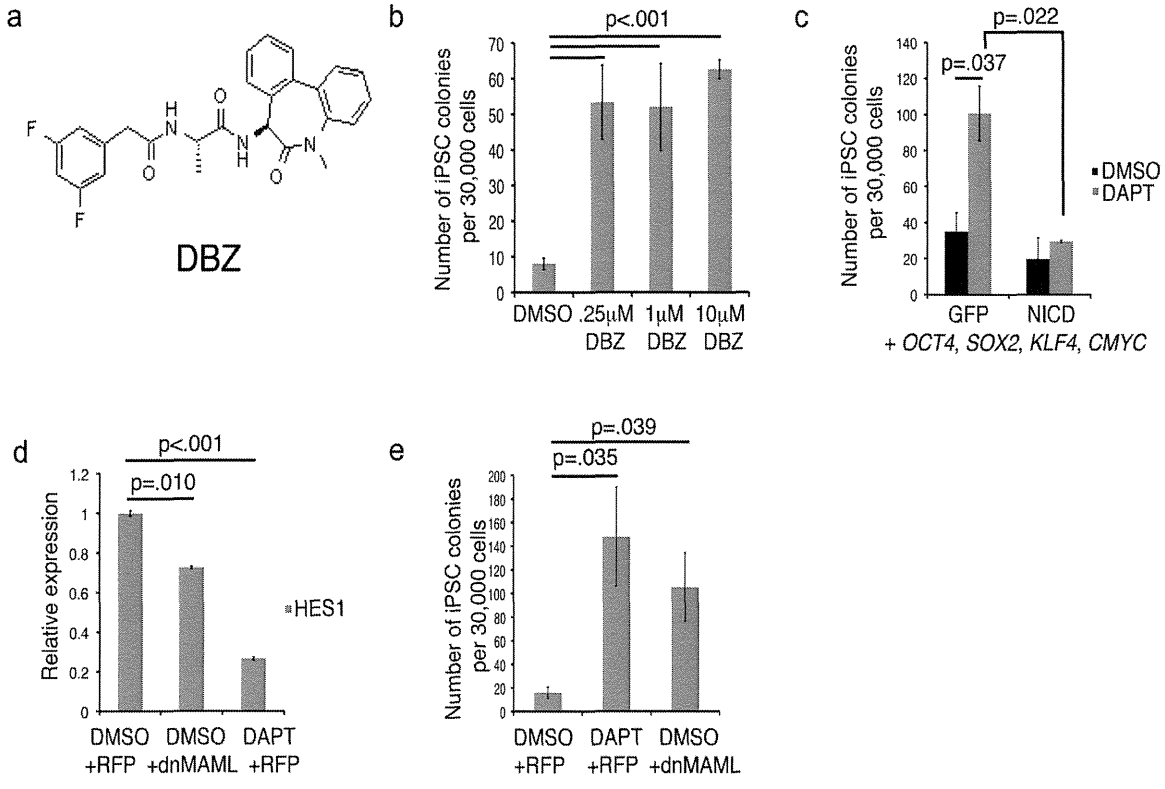

Figure 2. γ-secretase inhibition promotes reprogramming by blocking Notch signaling

a, Chemical structure of DBZ. **b**, The efficiency of NANOG+/TRA-1-81+ iPSC generation from human neonatal keratinocytes transduced with *OCT4, KLF4, SOX2*, and *CMYC* and treated with different concentrations of DBZ from days 1-18 post-transduction. **c**, The efficiency of NANOG+/ TRA-1-81+ iPSC generation from human neonatal keratinocytes transduced with *OCT, SOX2, KLF4*, and *CMYC* and GFP or NOTCH ICD and treated with DMSO or 10 μM DAPT from days 1-18 post-transduction. Cells were transduced with NOTCH ICD or GFP lentivirus 1 day after transduction with the reprogramming factors. **d**, qPCR analysis of expression levels of NOTCH-dependent gene HES1 in human neonatal keratinocytes transduced with dominant-negative MASTERMIND-LIKE-1 (*dnMAML*) or RFP. **e**, The efficiency of NANOG+/TRA-1-81+ iPSC generation from human neonatal keratinocytes transduced with *OCT, SOX2, KLF4*, and *CMYC* and RFP or *dnMAML* and treated with DMSO or 10 μM DAPT from days 1-18 post-transduction. For all experiments, error bars represent the standard deviation between two or three biological replicates and statistical significance was determined using a two-tailed homoscedastic Student's t-test.

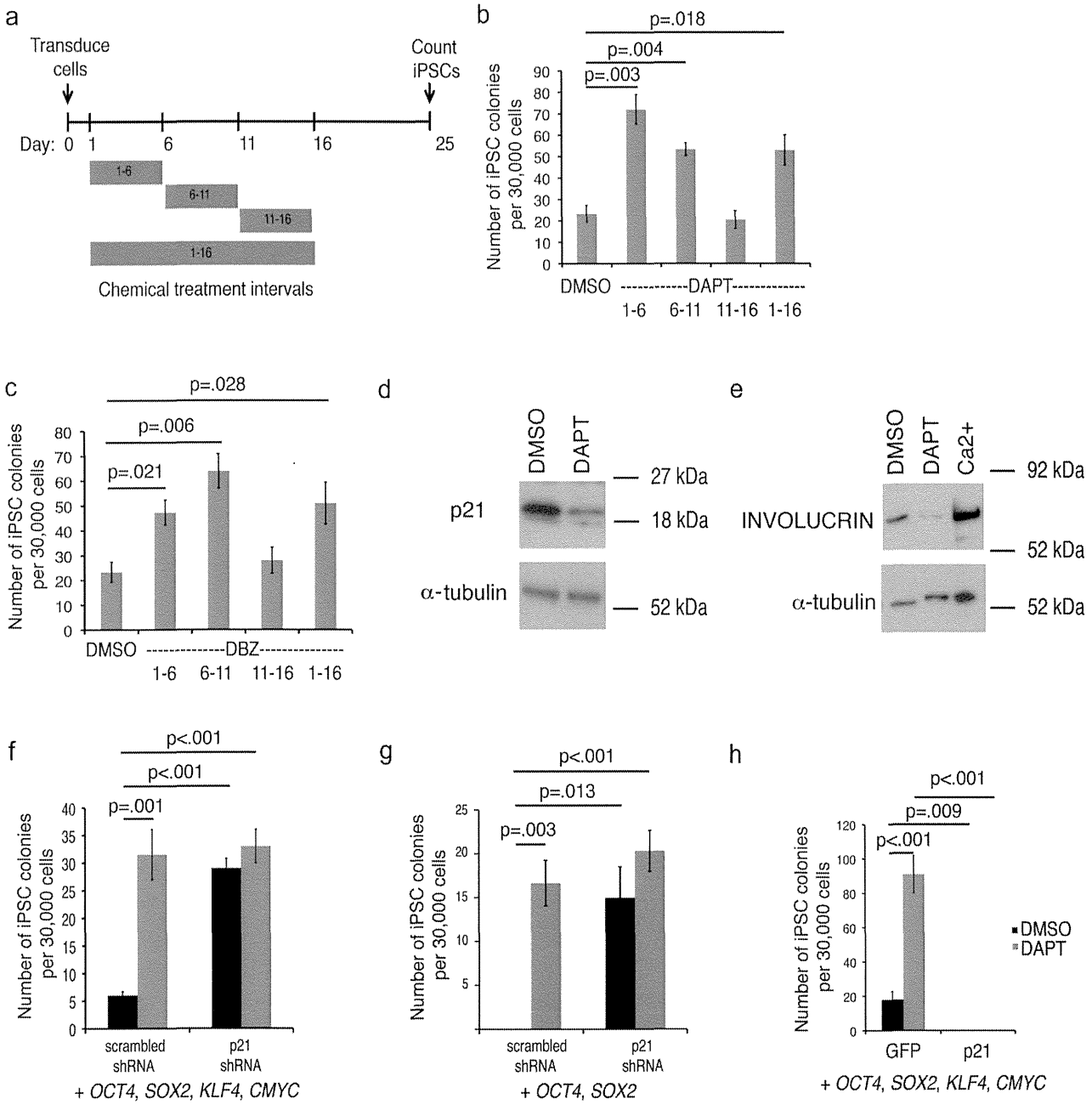

Figure 3. Notch inhibition promotes keratinocyte reprogramming by suppressing p21

a, Schematic of the DAPT treatment time course on human neonatal keratinocytes. **b**, Efficiency of NANOG+/TRA-1-81+ iPSC generation from human neonatal keratinocytes transduced with *OCT4, SOX2, KLF4*, and *CMYC* and treated with intervals of 10 μM DAPT or **c**, 2 μM DBZ. **d**, Western blot for p21 in human neonatal keratinocytes transduced with *OCT4* and *SOX2* and treated with DMSO or 10 μM DAPT. Full blot shown in Supplementary Figure 7c. **e**, Western blot for INVOLUCRIN in human neonatal keratinocytes treated with DMSO, 10 μM DAPT, or 1.2 mM calcium chloride for 6 days. Calcium was used as a positive control to induce keratinocyte differentiation. Full blot shown in Supplementary Figure 7d. **f**, Efficiency of NANOG+/TRA-1-81+ iPSC generation from human neonatal keratinocytes transduced with *OCT4, KLF4, SOX2*, and *CMYC* and a scrambled shRNA or a p21 shRNA at day 0 of reprogramming. DAPT was added at 10 μM.

g, Efficiency of NANOG+/TRA-1-81+ iPSC generation from human neonatal keratinocytes transduced with *OCT4* and *SOX2* and a scrambled shRNA control or a p21 shRNA at day 0 of reprogramming. DAPT was added at 2.5 μM. **h**, Efficiency of NANOG+/TRA-1-81+ iPSC generation from human neonatal keratinocytes transduced with *OCT, SOX2, KLF4*, and *CMYC* and GFP or p21 and treated with DMSO or 10 μM DAPT from days 1-18 post-transduction. For all experiments, error bars represent the standard deviation between two-three biological replicates and statistical significance was determined using a two-tailed homoscedastic Student's t-test.

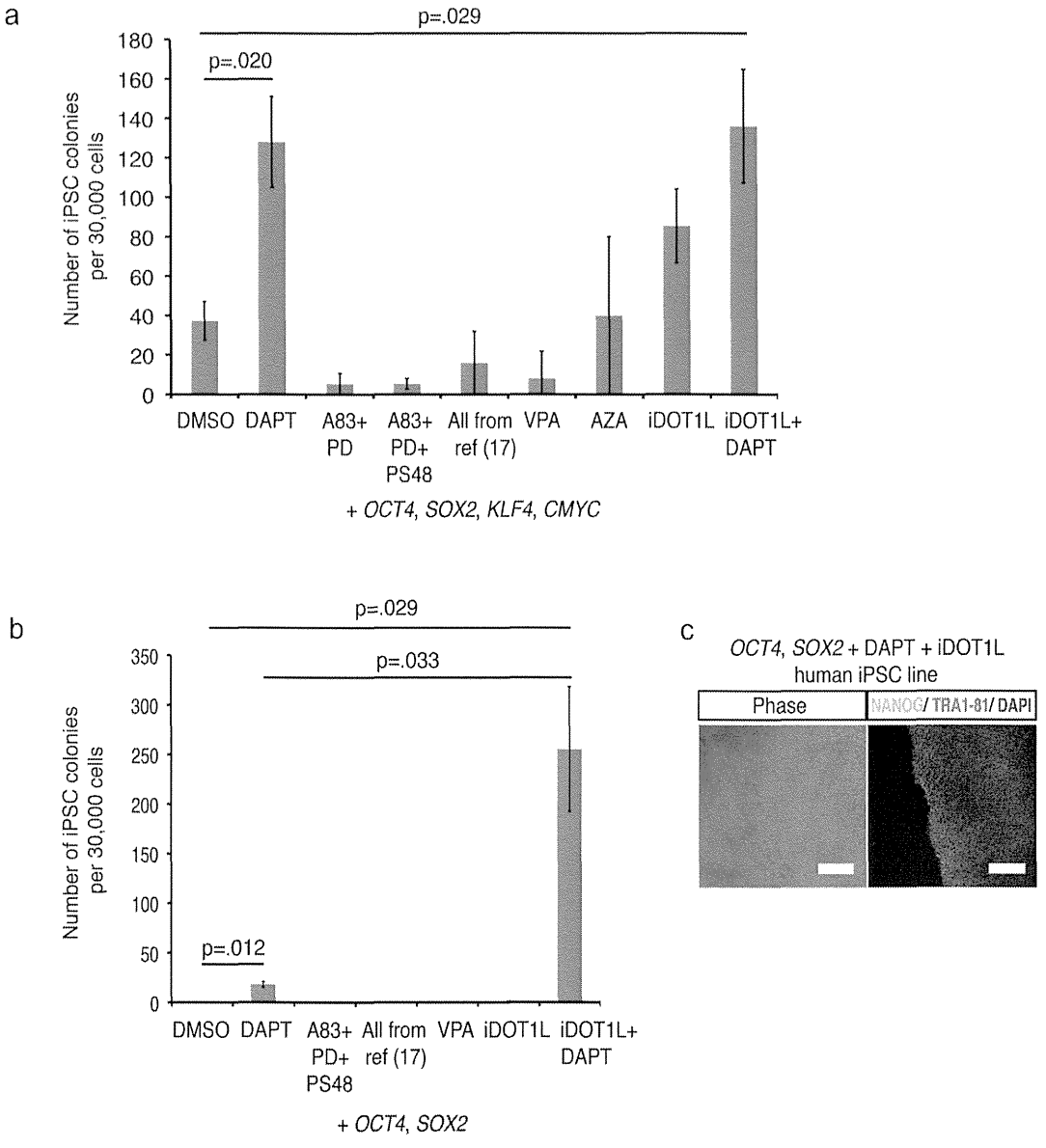

Figure 4. Highly efficient reprogramming with NOTCH and DOT1L inhibition

a, Comparison of NANOG+/TRA-1-81+ iPSC generation from *OCT4, SOX2, KLF4*, and *CMYC*-transduced human neonatal keratinocytes using 10 μM DAPT versus other published reprogramming chemicals. "A83" = A8301 (.5 μM), "PD" = PD0325901 (.5 μM), "All from ref (13)" = A8301 (.5 μM), PD0325901 (.5 μM), PS48 (5 μM), sodium butyrate (.25 mM), Parnate (2 μM), CHIR99021 (3 μM), "AZA" = 5-aza-cytidine (.5 μM), "VPA" = valproic acid (.5 mM), "iDOT1L" = EPZ004777 (3 μM). **b**, Comparison of NANOG+/TRA-1-81+ iPSC generation from *OCT4*- and *SOX2*-transduced human neonatal keratinocytes using 2.5 μM DAPT versus other published reprogramming chemicals. **c**, iPSC line generated from human neonatal keratinocytes using *OCT4, SOX2*, DAPT, and iDOT1L. scale bars = 100 μm. For all experiments, error bars represent the standard deviation between two-three biological replicates and statistical significance was determined using a two-tailed homoscedastic Student's t-test.

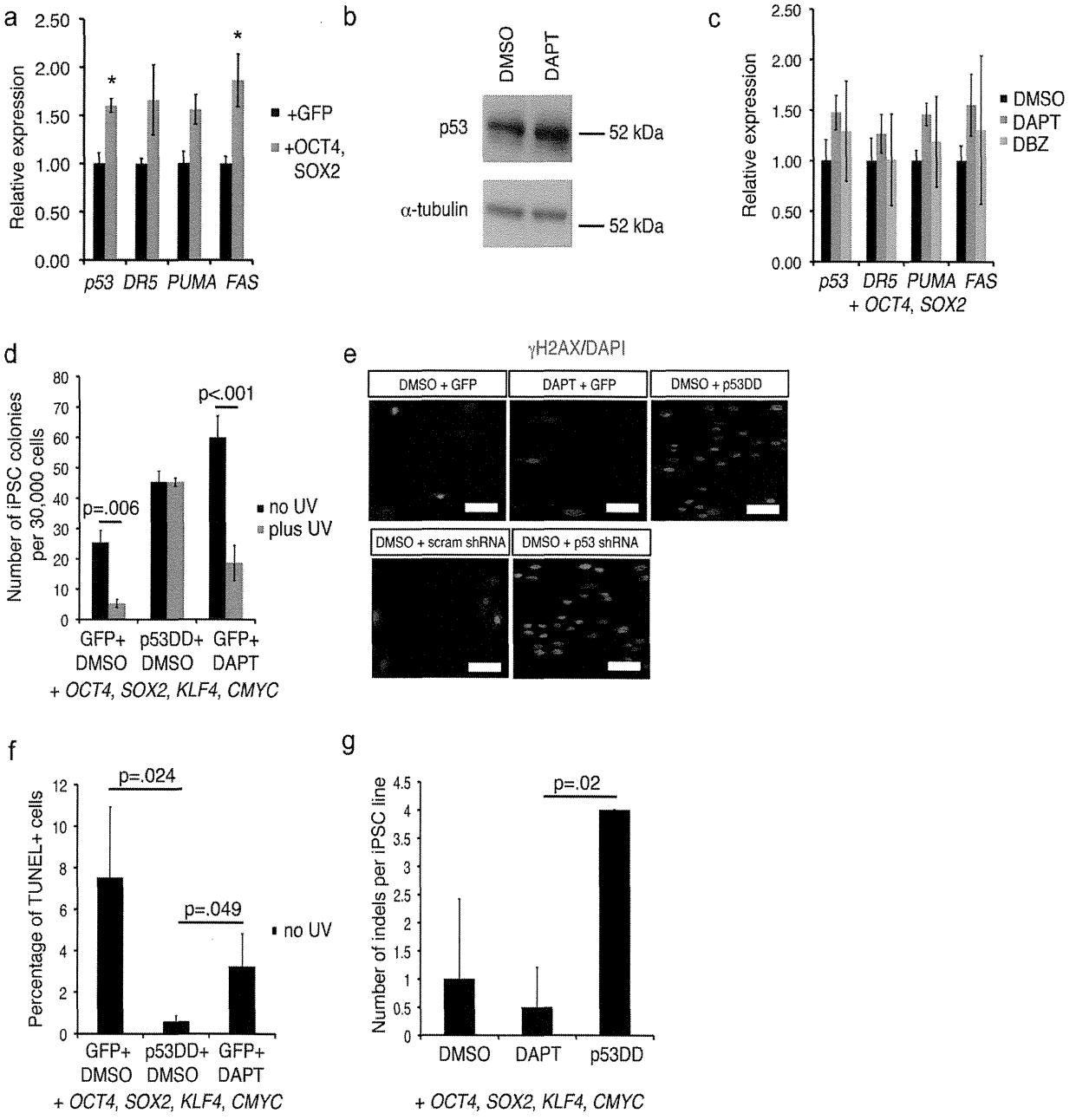

Figure 5. NOTCH inhibition suppresses p21 without reducing p53 activity

a, qPCR analysis of p53-dependent genes in human neonatal keratinocytes 3 days after transduction of GFP or *OCT4* and *SOX2*. **b**, Western blot of p53 levels in human neonatal keratinocytes with DMSO or 10 μM DAPT treatment for 3 days. Full blot shown in Supplementary Figure 7g. **c**, qPCR analysis of p53-dependent genes after 10 μM DAPT or 2 μM DBZ treatment for 3 days in *OCT4, SOX2*-transduced human keratinocytes. **d**, The efficiency of NANOG+/TRA-1-81+ iPSC generation in *OCT4, SOX2, KLF4*, and *CMYC*-transduced human neonatal keratinocytes transduced with p53DD or GFP with or without exposure to UV irradiation. **e**, γH2AX immunostaining in human neonatal keratinocytes 10 days after transduction with *OCT4, SOX2, KLF4*, and *CMYC* and treatment with DAPT, p53DD, or p53 shRNA. Scale bars = 50 μm. **f**, The percentage of TUNEL-positive cells in human neonatal keratinocyte reprogramming cultures with active or inactive p53 (p53DD

expression) 10 days after transduction with *OCT4, SOX2, KLF4*, and *CMYC*. **g**, The number of insertions or deletions (indels) per iPSC line derived under normal, DAPT, or p53DD conditions, as determined by array CGH. For all experiments, error bars represent the standard deviation between two biological replicates and statistical significance was determined using a two-tailed homoscedastic Student's t-test. * denotes significance p-value < .05.

Migita O, Maehara K, Kamura H, Miyakoshi K, Tanaka M, Morokuma S, Fukushima K, Shimamoto T, Saito S, Sago H, Nishihama K, Abe K, Nakabayashi K, **Umezawa A**, Okamura K, Hata K.	Compilation of copy number variants identified in phenotypically normal and parous Japanese women.	**J Hum Genet**.	59	326-331	2014
Yazawa T, Imamichi Y, Miyamoto K, **Umezawa A**, Taniguchi T.	Differentiation of mesenchymal stem cells into gonad and adrenal steroidogenic cells.	**World J Stem Cells**.	6	203-212	2014
Kawano N, Miyado K, Yoshii N, Kanai S, Saito H, Miyado M, Inagaki N, Odawara Y, Hamatani T, **Umezawa A**.	Absence of CD9 reduces endometrial VEGF secretion and impairs uterine repair after parturition.	**Sci Rep**.	4	4701	2014
Sugawara K, Hamatani T, Yamada M, Ogawa S, Kamijo S, Kuji N, Akutsu H, Miyado K, Yoshimura Y, **Umezawa A**.	Derivation of human decidua-like cells from amnion and menstrual blood.	**Sci Rep**.	4	4599	2014

Toyoda M, **Umezawa A**.	Stem cells bond our organs/tissues and engineering products.	**Circ J**.	78	1582-1583	2014
Kondo Y, Iwao T, Nakamura K, Sasaki T, Takahashi S, Kamada N, Matsubara T, Gonzalez FJ, Akutsu H, Miyagawa Y, Okita H, Kiyokawa N, Toyoda M, **Umezawa A**, Nagata K, Matsunaga T, Ohmori S.	An efficient method for differentiation of human induced pluripotent stem cells into hepatocyte-like cells retaining drug metabolizing activity.	**Drug Metab Pharmacokinet.**	29	237-243	2014
Tano K, Yasuda S, Kuroda T, Saito H, **Umezawa A**, Sato Y.	A novel in vitro method for detecting undifferentiated human pluripotent stem cells as impurities in cell therapy products using a highly efficient culture system.	**PLoS One**.	9	e110496	2014
Ninomiya E, Hattori T, Toyoda M, **Umezawa A**, Hamazaki T, Shintaku H.	Glucocorticoids promote neural progenitor cell proliferation derived from human induced pluripotent stem cells.	**Springerplus**.	3	527	2014

V. 研究成果の刊行物・別刷

Letters

OBSERVATION

Buruli Ulcer Successfully Treated With Negative-Pressure Wound Therapy

Buruli ulcer (BU) is a slowly progressive lesion with local necrosis caused by *Mycobacterium ulcerans*.[1] It is mostly seen in tropical areas,[2,3] and the lack of awareness of BU in nonendemic areas sometimes leads to diagnostic delay. Significant delay places patients at risk of more extensive disease. Negative-pressure wound therapy (NPWT) is considered to be a great alternative because it accelerates wound healing. Herein, we report an advanced case of BU successfully treated with NPWT.

Report of a Case | A woman in her 50s noticed a painless erythematous nodule, 1.0 cm in diameter, on the right ankle 4 months before her initial visit to our hospital. The patient had no history of traveling abroad but had been working in a vegetable field for the previous 9 months. She was diagnosed with pyoderma gangrenosum by a local dermatologist and prescribed oral cephem antibiotics and betamethasone (1 mg/d) for 2 months. However, the lesion grew, and she was referred for further evaluation.

Physical examination revealed a necrotic, ulcerative lesion, 10.0 × 5.5 cm, on the right ankle. Acid-fast bacilli were detected with Ziehl-Neelsen staining in smear specimens from the ulcer, though no pathogenic bacteria had been found by repeated cultures during the previous 4 months. By polymerase chain reaction (PCR), we confirmed the presence of insertion sequence (IS) *2404* in the DNA extracted from paraffin-embedded sections of the skin biopsy specimen, and it raised the possibility of *M ulcerans* or *M ulcerans* subspecies *shinshuense* as the causative organism (**Figure 1**A).

Then, we analyzed mycolactone-producing genes in the virulence plasmid pMUM001 from bacteria cultured from the wound. The PCR analysis showed the characteristic features of *M ulcerans* subspecies *shinshuense*, ie, only the serine/threonine protein kinase gene *MUP011* (479 base pairs) was not detected among mycolactone-producing genes in pMUM001 (Figure 1B). Thus, we established the final diagnosis of BU caused by *M ulcerans* subspecies *shinshuense*, and treatment was begun, adjusted to her low body weight of 38.4 kg, with clarithromycin (600 mg/d), rifampicin (450 mg/d), and levofloxacin (500 mg/d).

We regard the date when the specific treatment for BU was started as day 1. The lesion was larger than 15.0 cm in diameter at that time (**Figure 2**A). Since it seemed difficult to heal the lesion completely with only antibiotics, she was given surgical debridement on day 20. The ulcer had a necrotic bed, with the Achilles tendon and the calcaneal bone exposed (Figure 2B). We started NPWT with V.A.C. Therapy System (Kinetics Concepts Inc [KCI]) as a pretreatment for skin grafting on day 42. The vacuum suction was

Figure 1. Genetic Analysis by Polymerase Chain Reaction (PCR) Targeting *IS2404* and Virulence Plasmid pMUM001

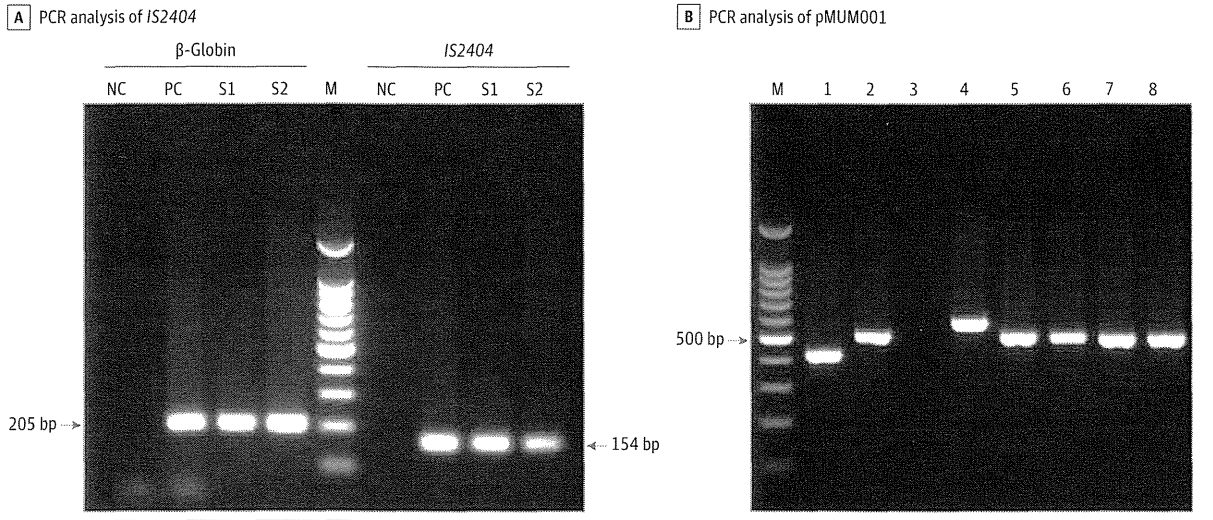

A, Under PCR analysis of *IS2404*, the biopsy specimen was found to be strongly positive for the 154-bp product, which raised the possibility of *Mycobacterium ulcerans* or *M ulcerans* subspecies *shinshuense* as the causative organism. Lane M represents a 100-base pair (bp) ladder marker; lane NC, a negative control; lane PC, a positive control; lane S1, a DNA sample extracted from paraffin-embedded skin (patient) before antibiotic use; lane S2, a DNA sample extracted from paraffin-embedded skin (patient) after antibiotic use. B, Under PCR analysis of virulence plasmid pMUM001, only lane 3 was found to be negative. These results clearly indicate the diagnosis of Buruli ulcer caused by *M ulcerans* subspecies *shinshuense*. Lane M represents a 100-bp ladder marker; lane 1, *repA* (413 bp); lane 2, *parA* (501 bp); lane 3, the serine/threonine protein kinase gene *MUP011* (479 bp); lane 4, a loading domain of *mls* (560 bp); lane 5, an acyltransferase domain of *mls* (504 bp); lane 6, the *rep* type II thioesterase gene (500 bp); lane 7, the *rep* type III ketosynthase gene (496 bp); and lane 8, the *rep P450* hydroxylase gene (500 bp).

Figure 2. Time Series of the Clinical Features of Buruli Ulcer (BU)

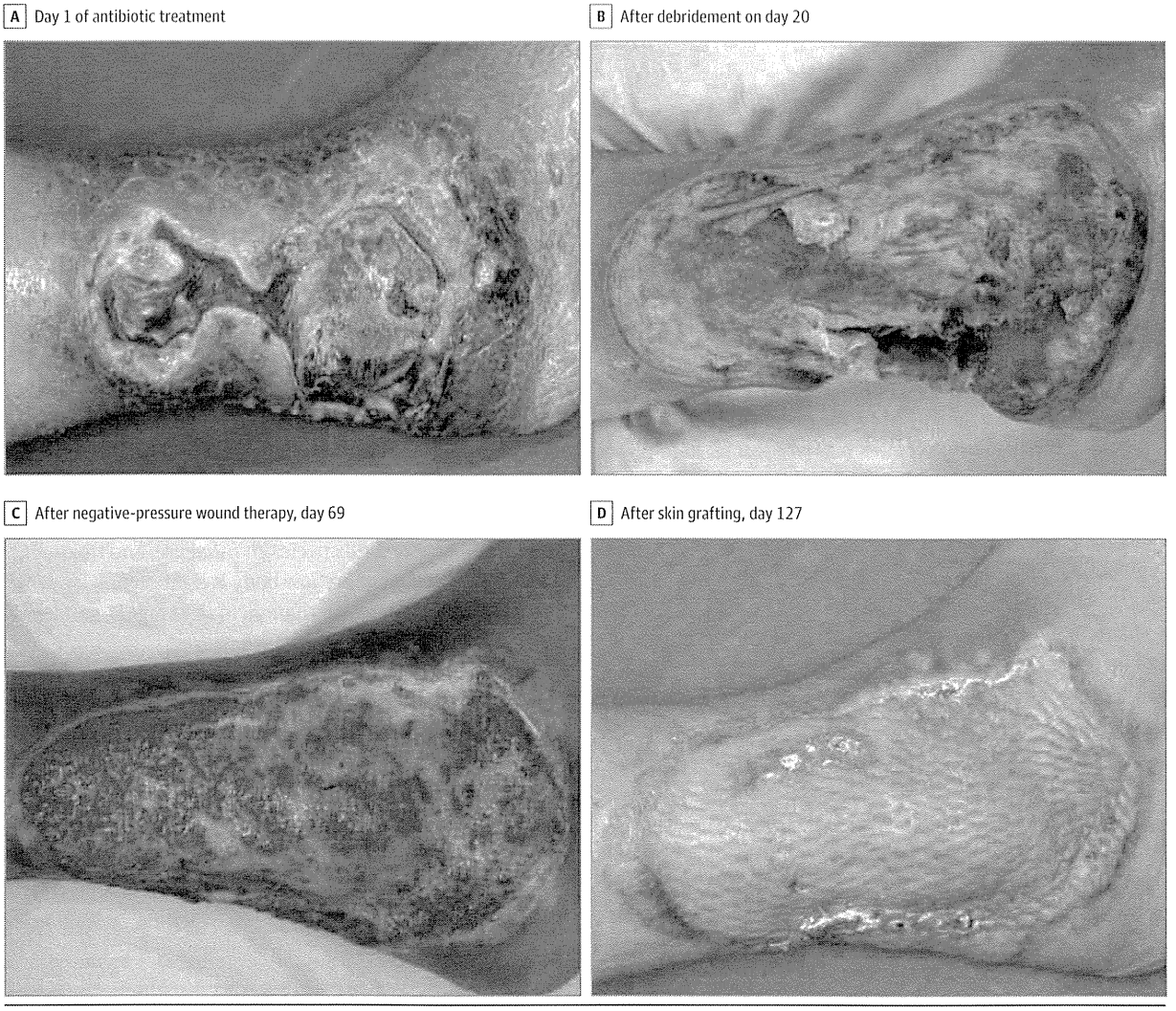

A, Painful ulceration with necrotic tissue surrounded by erythema on the right ankle on day 1 of BU-specific antibiotic treatment. B, The ulcer after radical debridement on day 20. The Achilles tendon and the calcaneal bone are exposed, and the articular capsule of the ankle joint has been destroyed. C, After negative-pressure wound therapy treatment, red granulation tissue covers the ulcer bed on day 69. D, The well-preserved skin graft completely encloses the lesion on day 127.

maintained at 125 mm Hg, and the wound dressings were changed every third day for 24 days. By day 69, good granulation tissue covered the ulcer bed (Figure 2C). A mesh skin graft was successfully engrafted on day 78. By day 127, the ulcer was completely healed, and she was able to walk again by herself (Figure 2D). Treatment with antibiotics was continued throughout the 4-month treatment course.

Discussion | Buruli ulcer should be considered in patients who present with chronic refractory ulcers or atypical cellulitis unresponsive to standard treatment. Its diagnosis relies primarily on PCR methods,[4] and PCR targeting of *IS2404* is a highly sensitive and specific diagnostic test (sensitivity and specificity >90%).[5]

In this case, although the lesion extended deeply and required radical debridement, we were able to avoid amputation and achieve good wound healing by wound bed preparation with NPWT, which increases wound blood flow and granulation tissue growth and decreases local edema and bacterial flora at the wound site.[6] Portable NPWT treatment devices are adaptable for outpatients and also can be used in developing countries. This treatment outcome suggests that NPWT might be appropriate for treatment of advanced BU cases.

Chiaki Murase, MD
Michihiro Kono, MD, PhD
Kazue Nakanaga, PhD
Norihisa Ishii, MD, PhD
Masashi Akiyama, MD, PhD

Author Affiliations: Department of Dermatology, Nagoya University Graduate School of Medicine, Aichi, Japan (Murase, Kono, Akiyama); Leprosy Research Center, National Institute of Infectious Diseases, Tokyo, Japan (Nakanaga, Ishii).

Corresponding Author: Michihiro Kono, MD, PhD, Department of Dermatology, Nagoya University Graduate School of Medicine, 65 Tsurumai-cho, Showa-ku, Nagoya-shi, Aichi 466-8550, Japan (miro@med.nagoya-u.ac.jp).

Published Online: June 24, 2015. doi:10.1001/jamadermatol.2015.1567.

Conflict of Interest Disclosures: None reported.

Additional Contributions: The authors thank Takaaki Matsumoto, MD, PhD, Kenji Yokota, MD, and Yoshie Hasegawa, MD, Department of Dermatology, Nagoya University Graduate School of Medicine, for performing the surgical procedures described herein. These persons received no compensation for their contributions beyond the normal course of their employment.

1. World Health Organization. *Treatment of* Mycobacterium ulcerans *Disease (Buruli Ulcer): Guidance for Health Workers.* Geneva, Switzerland: World Health Organization; 2012.

2. O'Brien DP, Comte E, Serafini M, et al. The urgent need for clinical, diagnostic, and operational research for management of Buruli ulcer in Africa. *Lancet Infect Dis*. 2014;14(5):435-440.

3. World Health Organization. *Working to Overcome the Global Impact of Neglected Tropical Diseases: First WHO Report on Neglected Tropical Diseases.* Geneva, Switzerland: World Health Organization; 2010.

4. Nakanaga K, Ishii N, Suzuki K, et al. "*Mycobacterium ulcerans* subsp. *shinshuense*" isolated from a skin ulcer lesion: identification based on 16S rRNA gene sequencing. *J Clin Microbiol*. 2007;45(11):3840-3843.

5. World Health Organization. *Laboratory Diagnosis of Buruli Ulcer: A Manual For Health Care Providers.* Geneva, Switzerland: World Health Organization; 2014.

6. Saaiq M, Hameed-Ud-Din, Khan MI, Chaudhery SM. Vacuum-assisted closure therapy as a pretreatment for split thickness skin grafts. *J Coll Physicians Surg Pak*. 2010;20(10):675-679.

Journal of Dermatological Science xxx (2015) xxx–xxx

Contents lists available at ScienceDirect

Journal of Dermatological Science

journal homepage: www.jdsjournal.com

Lymphatic flow is mostly preserved after sentinel lymph node biopsy in primary cutaneous malignant melanoma

Kenji Yokota, Masaki Sawada, Takaaki Matsumoto, Yoshie Hasegawa, Michihiro Kono, Masashi Akiyama *

Department of Dermatology, Nagoya University Graduate School of Medicine, Nagoya, Japan

ARTICLE INFO

Article history:
Received 22 December 2014
Received in revised form 16 February 2015
Accepted 17 February 2015

Keywords:
Adjuvant therapy
Interferon
Lymphatic flow
Malignant melanoma
Near-infrared
Sentinel lymph node

ABSTRACT

Background: Knowledge of changes in lymphatic flow after sentinel lymph node biopsy (SLNB) is important for the development of strategies for postoperative adjuvant therapy in malignant melanoma.
Objectives: 41 patients (22 males and 19 females; average age: 67.0 ± 24.0 years) with primary cutaneous malignant melanoma (PCMM) participated in the present study. The primary tumor sites were the upper extremities (9 patients), the lower extremities (20 patients), the trunk (11 patients) and the scalp (1 patient). The tumor thicknesses of the PCMM lesions were from 0.5 mm to 9.0 mm (average: 3.3 ± 2.5 mm). All the participants underwent wide local excision and SLNB.
Methods: We studied lymphatic flow before and after SLNB by near-infrared (NIR) imaging in all 41 cases. In addition, we performed NIR imaging of lymphatic flow after the lymph node dissection in one case with sentinel lymph node (SLN) metastasis.
Results: Almost no changes in lymphatic flow were seen in 38 of the 41 patients (92.7%) after SLNB. Only in 3 patients (7.3%), one with SLN metastasis and the other two without SLN metastasis, was apparent alteration in the lymphatic flow observed after SLNB. Of the 16 patients without SLN metastasis, only 3 patients showed recurrence of the tumors. Interestingly, 1 of the 2 patients without SLN metastasis but with lymphatic flow alteration had recurrence (regional lymph node metastasis) of the melanoma, whereas only 2 of the 14 patients without SLN metastasis or lymphatic flow alteration had recurrence, 1 with regional lymph node metastasis and the other with distant lymph node metastasis. In 1 case, we re-examined the lymphatic flow after regional lymph node dissection and the lymphatic flow was found to be dramatically changed.
Conclusion: We clearly demonstrated that SLNB has only a minimal effect on lymphatic flow. The present results suggest that SLNB does not increase the risk of local recurrence/in-transit metastasis and may support the efficacy of post-SLNB local adjuvant injection to prevent local recurrence and in-transit metastasis.

1. Introduction

Revealing the extent and patterns of changes in lymphatic flow after sentinel lymph node biopsy (SLNB) is essential for the development of strategies for postoperative adjuvant therapy of cutaneous malignant tumors, including primary cutaneous malignant melanoma (PCMM). It is apparent that SLNB results in less tissue damage than that for regional lymph node dissection [1]. However, information on lymphatic flow changes after SLNB has been limited.

Until recently, most imaging studies on human lymphatic flow have employed lymphoscintigraphy [2]. Studies by Celebioglu et al. [1] of lymph drainage in the arms after SLNB and after axillary lymph node dissection by lymphoscintigraphy revealed that lymph drainage was less affected by SLNB than by axillary lymph node dissection. However, lymphoscintigraphy is not sufficiently

Abbreviations: ICG, indocyanine green; NIR, near-infrared; PCMM, primary cutaneous malignant melanoma; SLN, sentinel lymph node; SLNB, sentinel lymph node biopsy.

* Corresponding author at: Department of Dermatology, Nagoya University Graduate School of Medicine, 65 Tsurumai-cho, Showa-ku, Nagoya 466-8550, Japan. Tel.: +81 52 744 2314; fax: +81 52 744 2318.
E-mail address: makiyama@med.nagoya-u.ac.jp (M. Akiyama).

http://dx.doi.org/10.1016/j.jdermsci.2015.02.011
0923-1811/